In situ laser heating and radial synchrotron x-ray diffraction in a diamond anvil cell

Martin Kunz and Wendel A. Caldwell
Advanced Light Source, Lawrence Berkeley Laboratory, Berkeley, California 94720

Lowell Miyagi and Hans-Rudolf Wenk
Department of Earth and Planetary Science, University of California, Berkeley, California 94720

(Received 27 April 2007; accepted 23 May 2007; published online 29 June 2007)

We report a first combination of diamond anvil cell radial x-ray diffraction with *in situ* laser heating. The laser-heating setup of ALS beamline 12.2.2 was modified to allow one-sided heating of a sample in a diamond anvil cell with an 80 W yttrium lithium fluoride laser while probing the sample with radial x-ray diffraction. The diamond anvil cell is placed with its compressional axis vertical, and perpendicular to the beam. The laser beam is focused onto the sample from the top while the sample is probed with hard x-rays through an x-ray transparent boron-epoxy gasket. The temperature response of preferred orientation of (Fe,Mg)O is probed as a test experiment. Recrystallization was observed above 1500 K, accompanied by a decrease in stress. © *2007 American Institute of Physics.* [DOI: 10.1063/1.2749443]

I. INTRODUCTION

Elastic x-ray diffraction is used routinely to probe structure and physical properties of material at conditions as they occur in the interior of planets. A convenient method is to load samples into diamond anvil cells (DACs), apply pressure, and simultaneously heat with an infrared laser while probing with highly brilliant synchrotron x-rays. The sample is often embedded in a soft pressure medium (e.g., noble gas, MgO) to approximate hydrostatic pressure conditions.[1] For many applications it is desirable to avoid deviatoric stresses as much as possible. But the behavior of a material under nonhydrostatic pressure can also provide valuable information on physical properties, in particular, the anisotropy of elastic properties and plastic deformation. Many materials that are brittle at ambient conditions become ductile at high pressure. In this case it is convenient to use a radial diffraction geometry with the diamond axis perpendicular to the incident x-ray beam, rather than axial diffraction geometry (Fig. 1).[2] The x-ray beam passes through an x-ray transparent gasket and the sample. In this case, for any given lattice plane, crystallites with the diffraction vector subparallel to the DAC axis probe a different stress than crystallites with the diffraction vector subparallel to the gasket plane. Elastic deformation of crystals is expressed in changes in d spacings and according shifts in diffraction peaks. Probing a powder under nonhydrostatic stress conditions in radial diffraction geometry therefore leads to elliptic Debye rings. Plastic deformation by dislocation glide and mechanical twinning produces rotations of crystals, which causes intensity variations of the Debye ellipses along their azimuthal angle. These effects can be used to determine elastic properties as well as deformation mechanisms. This type of experiments has been conducted on minerals such as periclase,[3] perovskite,[4] and postperovskite,[5] all at room temperature. Obviously deformation in the earth occurs at much higher temperature and the influence of temperature on deformation patterns needs to be investigated to establish applicability of DAC laboratory experiments to earth conditions. This has so far not been possible.

Combining a radial diffraction diamond anvil cell with an internal heater is difficult as the metallic heating wire wrapped around the sample gasket obscures x-ray access in the radial direction.[6,7] Laser heating a radial diffraction cell with an infrared (IR) laser has so far been hampered by the fact that all current *in situ* laser heating facilities at synchrotron beamlines are arranged for axial diffraction with the laser heating optics parallel to the x-ray beam. Laser heating of a sample in a DAC can only be achieved through the diamonds. The combination of radial diffraction with laser heating thus requires a modification of the *in situ* laser setup

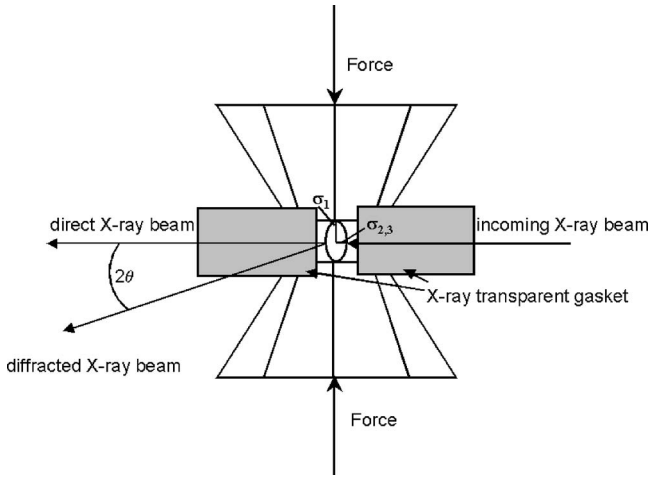

FIG. 1. Schematic drawing of radial diffraction geometry. The incoming x-ray beam is perpendicular to the direction of the applied force and thus to σ_1 of the stress tensor (stress ellipsoid with principal axis is shown at sample position).

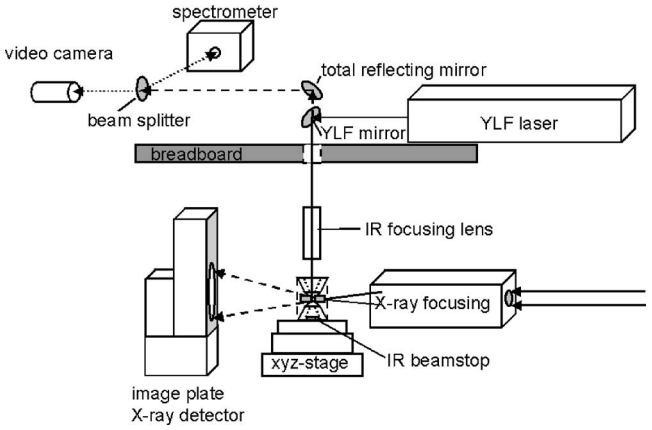

FIG. 2. Schematic of experimental setup for one-sided *in situ* laser heating of a diamond anvil cell in radial diffraction geometry.

to allow for a perpendicular arrangement of the IR laser and the x-ray beam, respectively. The high-pressure beamline HPCAT at the Advanced Photon Source (APS) is constructing an elaborate setup for double-sided laser heating while doing radial diffraction.[8] Here we present a simpler modification at beamline 12.2.2 of the Advanced Light Source (ALS) allowing for one-sided heating of a sample in a diamond anvil cell conducting *in situ* x-ray diffraction in radial geometry. As test sample for this pilot experiment we chose magnesiowuestite. The main reason was that deformation mechanisms of this cubic mineral with a simple diffraction pattern are reasonably understood[9,10] and the material was studied previously with DAC in radial diffraction.[11] Also, elastic properties are well known. The composition $Mg_{0.75}Fe_{0.25}O$ was chosen to have significant coupling with the IR laser. The plan was to induce preferred orientation at ambient temperature through nonhydrostatic compression and then follow *in situ* changes in the preferred orientation pattern during heating the sample up to ~1500 K.

II. EXPERIMENTAL PROCEDURE

Details on the source and optics of beamline 12.2.2 at ALS are given elsewhere.[12] For the present experiment, the x-ray beam was refocused from its primary focal spot of ~150 μm (h) × 90 μm (v) onto a 12 × 12 μm^2 spot using a pair of Kirkpatrick-Baez mirrors placed on the experimental table (Fig. 2). In order to combine one-sided laser heating with radial x-ray diffraction, the 12.2.2 laser heating setup[13] is modified as follows (Fig. 2): The silver coated carbon mirrors, which reflect the laser beam parallel to the x-ray beam into the diamond anvil cell, are removed. The DAC is mounted with the compressional axis vertical onto a holder covered with an IR absorbing ceramic serving as a laser beam stop underneath the DAC. This geometry allows us to focus the IR laser into the diamond anvil cell through the diamond window as it is directed down from the laser conditioning stage onto the x-ray table (Fig. 2). The cell is centered on the vertical rotation axis of the goniometer and the IR laser beam is subsequently aligned onto the rotation axis. As an IR laser beam we used an 80 W yttrium lithium fluoride (YLF) laser operated in the TEM01 mode (usable laser power of 50 W). The procedure to center the sample onto the rotation axis and accurately determine the sample to detector distance is described in Ref. 12. The sample to detector distance was calibrated using a LaB_6 standard with fitting routines as implemented in FIT2D.[14] To maximize absorption contrast during centering, the energy of the x-ray beam was lowered to 10 keV for the alignment process. Diffraction images were taken at 20 and 25 keV with a 5 min exposure time.

In axial geometry, the IR laser beam is aligned onto the x-ray beam by steering the laser beam with the motorized carbon mirror onto the previously aligned x-ray spot. The x-ray spot is "visualized" only indirectly through an x-ray absorption "map" of the gasket hole. Any prominent feature in this map serves as a reference point for the x-ray spot. This procedure is not possible in this setup because the remote controlled carbon mirrors are removed and therefore the viewing system is set up perpendicular to the x-ray beam rather than parallel to it. Therefore, the x-ray absorption map of the sample chamber cannot be transferred onto the visual image. To overcome this problem, a 10 μm Pt sphere pressed into the surface of a boron carbide pellet served as a

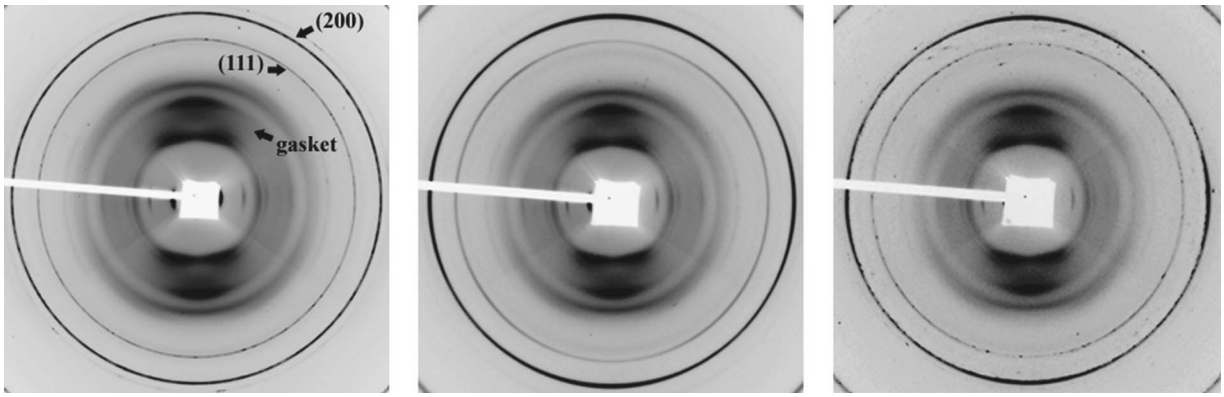

FIG. 3. (a) Radial diffraction image of $Mg_{0.75}Fe_{0.25}O$ taken at 20 keV at the start of the experiment. Image shows (111) and (200) peaks. The diffuse region at low angles is from the boron-kapton gasket. Pressure is 2.5 GPa. Image is somewhat spotty and there is little significant texturing. (b) Radial diffraction image of $Mg_{0.75}Fe_{0.25}O$ at 25 keV taken after compression to 28.5 GPa. The diffraction image is much smoother due to compaction of the sample and exhibits strong texture. (c) Radial diffraction image of $Mg_{0.75}Fe_{0.25}O$ at 25 keV taken during a 5 min heating period. Pressure is 27.8 GPa. The pattern is much spottier than Fig. 1(b) as a result of grain growth and recrystallization, but still has strong texture.

reference marker for the position of the x-ray beam in the horizontal direction. The high x-ray absorption of the Pt pellet allowed us to center it precisely onto the rotation axis and onto the x-ray beam. Once aligned onto the x-rays, its position as seen with the viewing system perpendicular to the x-ray beam served as a reference for the position of the x-ray beam. The IR laser beam was subsequently centered on the Pt sphere by manually adjusting the infrared mirrors, which are used to reflect the laser beam onto the focusing lens. Once x-rays and IR laser were aligned to cross path on the Pt pellet, the sample could be moved in order to heat and probe simultaneously any desired portion of the sample chamber. Visualizing and temperature measurement were set up on the downstream side analogous to the method used for axial diffraction.[13]

The sample[15] of composition $Mg_{0.75}Fe_{0.25}O$ was loaded into a two-stage kapton and boron-epoxy gasket (gasket hole of 80 μm) with no pressure medium in order to maximize the macroscopic deviatoric stress. No additional IR laser absorber was mixed with the sample, since the high Fe content of the Mg wuestite provided sufficient coupling with the IR laser. At the time of the experiment, the temperature measurement was not set up as yet. From the glow of the sample, we estimate to have achieved temperatures between 1500 and 2000 K.

Radial diffraction images were quantitatively analyzed for texture and lattice strains using the Rietveld method as implemented in the software package MAUD,[16] and first applied to synchrotron diffraction images by Ref. 17. Rietveld refinement with MAUD accounts for instrumental parameters such as beam center, detector tilt, peak shape, backgrounds, and azimuthal absorption. Once instrument parameters have been fitted, structural and microstructural parameters including differential stresses and texture may be refined. For refinements an angular 2θ range of 14.0°–20.0° at 20 keV was used for the image at the start of the experiment and a 2θ range of 11.5°–21.0° for images after compression and during heating.

Pressure was calibrated using a third order *P-V-T* Birch-Murnaghan equation of state and values of K_{T0}, K_{T0}', dK/dT, α_0, and α_1 from Ref. 18. The moment pole stress model using a bulk path geometric mean[19] (BPGeo) and elastic constants from Ref. 20 were used for the calculation of differential stresses. According to the geometry of radial diffraction experiments in DAC, the stress tensor was fixed such that $\sigma_{ij}=0$ for $i \neq j$, $\sigma_{11}=\sigma_{22}$, and $\sigma_{33}=-2\sigma_{11}$, where σ_{33} is the largest principal stress and is negative for compression. Textures were calculated using the tomographic E-WIMV algorithm, which is similar to the WIMV model.[21] For texture calculation cylindrical symmetry was imposed around the compression axis. The orientation distribution function (ODF) was given a resolution of 15° and the refined ODF was exported to BEARTEX (Ref. 22) and further smoothed with a 7.5° Gauss filter.

III. RESULTS AND DISCUSSION

Figure 3 shows radial diffraction images of $Mg_{0.75}Fe_{0.25}O$. The broad diffuse lines near the center of the image are diffraction from the kapton used in the gasket assembly. At the start of the experiment there is little texture and the image is slightly spotty [Fig. 3(a)]. After compression at ambient temperature the development of strong variations in azimuthal intensity becomes apparent and the diffraction is smoother and less spotty than at the start of the experiment due to fragmentation during compaction and deformation of the sample [Fig. 3(b)]. During a 5 min heating at ~1500 K the diffraction image becomes very spotty again due to grain growth and recrystallization [Fig. 3(c)]. The changes, particularly in lattice strains, are more obvious if the diffraction pattern with Debye ellipses is "unrolled" along the azimuthal angle using the cake routine of FIT2D,[14] Fig. 4. Figure 4(a) exhibits little distortion of diffraction lines due to lattice strains and little intensity variation along Debye ellipses [Figs. 3(a) and 4(a)]. Just after compression diffraction lines exhibit strong sinusoidal distortions due to lattice strains imposed by the DAC [Fig. 4(b)] as well as systematic intensity variations [Figs. 3(b) and 4(b)]. During

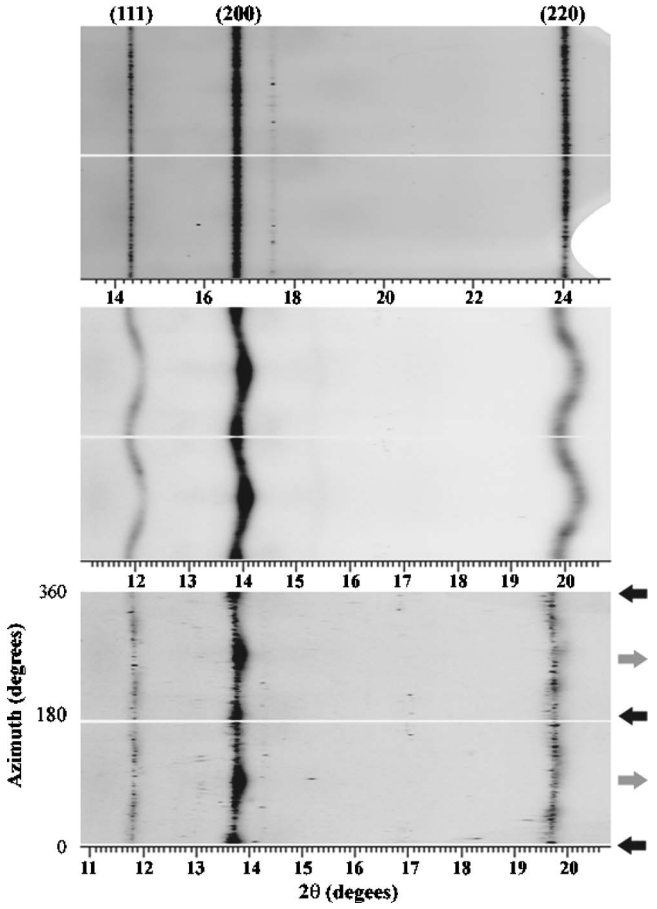

FIG. 4. Unrolled images of Fig. 3. Peaks are labeled and the compression direction is indicated by black arrows and the extension direction is indicated by gray arrows. (a) "Unrolled" image of Fig. 3(a). Lattice strain due to differential stress is not apparent as there is no deviation in peak position with azimuth. Texture is very weak and the pattern is spotty. (b) "Unrolled" image of Fig. 3(b). Here we observe the development of lattice strains due to high differential stresses. The compression direction is at an azimuthal angle of 90° and at 270°. Texture is quite evident as systematic azimuthal intensity variations along diffraction lines. (c) "Unrolled" image of Fig. 3(c). Lattice strains have relaxed due to heating and diffraction lines are relatively straight and undistorted. Recrystallization and grain growth resulting from heating cause the development of the spotty pattern.

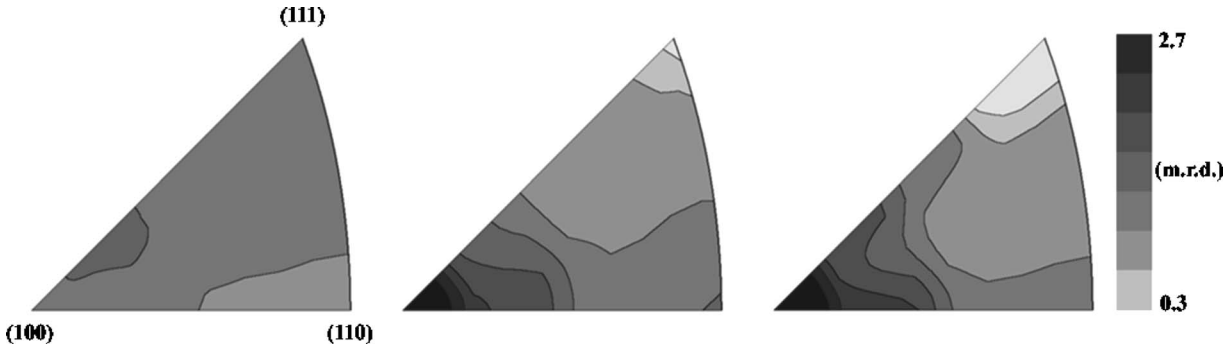

FIG. 5. Inverse pole figures showing texture results for $(Mg_{0.75}Fe_{0.25})O$. Projection is equal-area upper hemisphere with linear contours for all inverse pole figures shown. (a) Inverse pole figure of the compression direction at the start of the experiment (P=2.5 GPa). Texture is very weak as expected early in compression. (b) Inverse pole figure of the compression direction after room temperature compression to 28.3 GPa. A strong {100} texture maximum has developed with a small minimum at {111}. (c) Inverse pole figure during heating. Pressure is 27.8 GPa. The {100} texture maximum is slightly stronger present. Most notably the {111} minimum has become more depleted as a result recrystallization favoring the "softer" {100} orientations at the expense of the "hard" {111} orientations.

heating [Fig. 4(c)] diffraction lines straighten due to stress relaxation. However, diffraction lines appear to show two phases: one with straight spotty diffraction lines overlain by a smoother, broad, and more highly stressed set of diffraction lines [Fig. 4(c)]. This is due to thermal gradients within the DAC that result from the laser spot size being smaller than the sample chamber. Since the x-rays pass through the sample in the radial direction both "hot" and "cold" regions will be sampled.

These images were used to determine preferred orientation by analyzing them with the Rietveld method.[16] Texture results are represented as inverse pole figures in Figs. 5(a)–5(c) for the start of the experiment, just after compression and during heating. The inverse pole figures indicate the probability of finding a particular lattice plane perpendicular to the compression direction. Probabilities are given in multiples of random distribution (m.r.d.) where a random distribution has a m.r.d. value equal to 1 and a m.r.d. greater than 1 indicates a concentration of lattice planes perpendicular to the compression direction. Some additional information is given in Table I.

Upon compression to 28.3 GPa development of a strong {100} texture is observed [Fig. 5(b)] as well as the generation of significant lattice strains due to deviatoric stresses from compression. This is compatible with room temperature compression of magnesiowustite in previous DAC experiments.[3,11] Differential stresses also increase yielding an axial stress component t=4.44(1) GPa. The axial stress component t is commonly used as a lower bound estimate of the yield strength of a material and is equal to $-(3/2)\sigma_{33}$.

TABLE I. Summary of parameters from Rietveld refinement.

	Pressure (GPa)	a (Å)	t (GPa)	Texture min. (m.r.d.)	Texture max. (m.r.d.)
Start	2.5	4.24	0	0.78	1.30
Compressed	28.5	4.07	4.44(1)	0.02	3.46
High temperature	27.8[a]	4.12	1.41(1)	0.02	3.71

[a]Pressure calibrated assuming a temperature of 1500 K.

Our value of t=4.44(1) GPa at 28.3 GPa is somewhat higher than that measured in previous radial diffraction measurements on pure MgO.[3]

During heating a spotty pattern develops which is indicative of recrystallization and grain growth. Figure 5(c) shows an inverse pole figure obtained during heating. The {100} component has strengthened and the region around {111} has become more depleted in orientations. This texture change is compatible with recrystallization, as has been documented in isostructural halite, where a strong cube texture develops.[23] Polycrystal plasticity modeling suggests that during recrystallization grains that are plastically soft nucleate and then grow, replacing harder grains.[24] Orientations with {100} lattice planes perpendicular to the compression direction deform most easily and thus are most subject to recrystallization.[25] In MgO, like NaCl, room temperature compression yields a {100} maximum as a result of dominant {110}⟨1-10⟩ slip.[3,11,26] Upon recrystallization the hard {111} orientations become depleted while the {100} maximum strengthens.[24] This is what is observed during heating of $Mg_{0.75}Fe_{0.25}O$ in this experiment. The strong sinusoidal variations in peak position that were evident prior to heating relax and stresses drop to 1.41(1) GPa due to annealing. The unit cell parameters increase during heating from a value of a=4.07 Å to a=4.12 Å and pressure decreases to 27.8 GPa. This expansion of the unit cell is in part due to relaxation of differential stresses during heating which causes the slight pressure decrease observed here and it is also due to thermal expansion of the crystal lattice.

One of the prime applications of radial diffraction DAC experiments is to investigate deformation mechanisms and possible preferred orientation patterns of rocks in the deep earth (lower mantle, core). This is of utmost importance for a quantitative mineralogical and geodynamic interpretation of seismic information, the only direct observation of the interior of the planet. An obvious limitation in using ambient temperature results is that the temperature in the lower mantle is expected to be around 2000 K. It is therefore desirable to develop reliable heating methods for radial diffraction.

IV. FUTURE DEVELOPMENTS

Having shown that we can combine laser heating with a radial diffraction geometry, the next step will be to measure temperatures during x-ray diffraction while the sample is simultaneously under high pressure and at high temperature. Temperature can be measured by the spectroradiometric technique, wherein blackbody emission from the sample is imaged onto the entrance slit of a spectrometer.[27] The spectral range of measurement runs from 400 to 900 nm, but the data are typically fitted between 600 and 800 nm as that range reduces any errors introduced by chromatic aberration, while preserving a wide enough window for good fitting statistics to the Planck curves. In this technique one spatial dimension of the sample is preserved (along the entrance slit) giving a temperature profile through the entire heated part of the sample. The focusing optics of the experimental setup gives a hot spot that is typically 25 μm full width at half maximum (FWHM). The resolution of the image at the spectrometer gives approximately 2 μm pixel, so that temperature is measured at over a dozen neighboring positions on the sample. Temperatures between 1400 and 4000 K can be determined with this method.

A further improvement, which is being implemented, is the decoupling of laser alignment from image alignment by motorizing the IR mirrors, which direct the IR beam onto the focusing lenses. This will allow us to remotely steer the IR beam onto the x-ray beam also in radial geometry where we operate without the carbon mirrors normally used for IR-beam adjustment.

As discussed above, one of the fundamental problems of this method is the fact that with the x-ray beam perpendicular to the IR laser beam, we simultaneously probe hot material in the laser focus spot as well as cold sample surrounding it. To a certain extent this can be resolved by refining cold and hot samples as separate phases in the Rietveld analysis. The ultimate goal, however, is to minimize this effect experimentally. We plan to do this on one hand by reducing the sample chamber in the boron gasket. At the same time, we aim at increasing the laser spot size. Since this reduces the power density, the maximal size of the hot spot is limited by the laser power. With the 80 W YLF laser at ALS temperatures above 1500 K can be reached for a spot size of $\sim$50 μm. With a more powerful heating laser this can be improved.

In situ observation of anisotropy changes in radial diffraction geometry at pressure and temperature brings us one step closer to reproducing conditions in the deep earth. A future project, under development at ALS, is to add a motorized system to change pressure and stress at temperature to follow *in situ* the deformation history of a sample as in large volume apparatus such as D-DIA but at much higher pressures.

ACKNOWLEDGMENTS

The Advanced Light Source is supported by the Director, Office of Science, Office of Basic Energy Sciences, Materials Sciences Division, of the U.S. Department of Energy under Contract No. DE-AC03-76SF00098 at Lawrence Berkeley National Laboratory and University of California, Berkeley, California. COMPRES, the Consortium for Materials Properties Research in Earth Sciences under NSF Cooperative Agreement No. EAR 01-35554, supported this project through funding of two of the authors (M.K. and W.A.C), as well as crucial beamline equipment. Two of the authors (H.-.R. W. and L.M.) acknowledge support from CDAC and NSF (EAR 0337006). This document was prepared as an account of work sponsored by the United States Government. While this document is believed to contain correct information, neither the United States Government nor any agency thereof, nor The Regents of the University of California, nor any of their employees, makes any warranty, express or implied, or assumes any legal responsibility for the accuracy, completeness, or usefulness of any information, apparatus, product, or process disclosed, or represents that its use would not infringe privately owned rights. Reference herein to any specific commercial product, process, or service by its trade name, trademark, manufacturer, or otherwise, does not necessarily constitute or imply its endorsement, recommendation, or favoring by the United States Government or any agency thereof, or The Regents of the University of California. The views and opinions of authors expressed herein do not necessarily state or reflect those of the United States Government or any agency thereof or The Regents of the University of California.

[1] R. T. Downs, C. S. Zha, T. S. Duffy, and L. W. Finger, Am. Mineral. **81**, 51 (1996).
[2] A. K. Singh, C. Balasingh, H. K. Mao, R. J. Hemley, and J. F. Shu, J. Appl. Phys. **83**, 7567 (1998).
[3] S. Merkel, H. R. Wenk, J. F. Shu, G. Y. Shen, P. Gillet, H. K. Mao, and R. J. Hemley, J. Geophys. Res., [Solid Earth] **107**, 2271 (2002).
[4] H. R. Wenk, S. Speziale, A. K. McNamara, and E. J. Gamero, Earth Planet. Sci. Lett. **245**, 302 (2006).
[5] S. Merkel, A. Kubo, L. Miyagi, S. Speziale, T. S. Duffy, H.-K. Mao, and H.-R. Wenk, Science **311**, 644 (2006).
[6] L. Dubrovinsky, N. Dubrovinskaia, H. Annersten, E. Halenius, and H. Harryson, Eur. J. Mineral. **13**, 857 (2001).
[7] A. E. Gleason, S. Parry, A. Pawley, and S. M. Clark, Am. Mineral. (submitted).
[8] Y. Meng, G. Shen, and H.-K. Mao, J. Phys.: Condens. Matter **18**, S1097 (2006).
[9] M. S. Paterson and C. W. Weaver, J. Am. Ceram. Soc. **53**, 463 (1970).
[10] I. Stretton, F. Heidelbach, S. Mackwell, and F. Langenhorst, Earth Planet. Sci. Lett. **194**, 229 (2001).
[11] C. E. Tommaseo, J. Devine, S. Merkel, S. Speziale, and H.-R. Wenk, Phys. Chem. Miner. **83**, 84 (2006).
[12] M. Kunz *et al.*, J. Synchrotron Radiat. **12**, 650 (2005).
[13] W. A. Caldwell *et al.*, EOS Transactions AGU Fall Meeting, 2005 (unpublished), Vol. 86.
[14] A. P. Hammersley, ESRF Internal Report, Report No. ESRF97HA02T, 1997 (unpublished).
[15] L. J. Bonczar and E. K. Graham, J. Geophys. Res. **87**, 1061 (1982).
[16] L. Lutterotti, S. Matthies, H.-R. Wenk, A. S. Shultz, and A. J. W. Richardson, J. Appl. Phys. 81, 594 (1997).
[17] I. Lonardelli, H. R. Wenk, L. Lutterotti, and M. Goodwin, J. Synchrotron Radiat. **12**, 354 (2005).
[18] W. Westrenen *et al.*, Phys. Earth Planet. Inter. **151**, 163 (2005).
[19] S. Matthies, H. G. Priesmeyer, and M. R. Daymond, J. Appl. Crystallogr. **34**, 585 (2001).
[20] J. M. Jackson, S. Sinogeikin, S. D. Jacobsen, H. J. Reichmann, S. Mackwell, and J. D. Bass, J. Geophys. Res., [Solid Earth] **111**, B09203 (2006).
[21] S. Matthies and G. W. Vinel, Phys. Status Solidi B **112**, K115 (1982).
[22] H. R. Wenk, S. Matthies, J. Donovan, and D. Chateigner, J. Appl. Crystallogr. **31**, 262 (1998).

[23] W. Skrotzki and P. Welch, Tectonophysics **99**, 47 (1983).
[24] H. R. Wenk, G. Canova, Y. Brechet, and L. Flandin, Acta Mater. **45**, 3283 (1997).
[25] H. R. Wenk, G. Canova, A. Molinari, and H. Mecking, Acta Metall. **37**, 2017 (1989).
[26] R. A. Lebensohn, P. R. Dawson, H. M. Kern, and H. R. Wenk, Tectonophysics **370**, 287 (2003).
[27] D. L. Heinz and R. Jeanloz, in High-Pressure Research in Mineral Physics, edited by M. Manghnani and Y. Syono (American Geophyical Union, Washington, DC, 1984), pp. 113–127.